Magic Structures and Quantum Conductance of [110] Silver Nanowires

Dayong Cheng,[1] Woo Youn Kim,[1,*,†] Seung Kyu Min,[1] Tashi Nautiyal,[1,2] and Kwang S. Kim[1,*,‡]

[1]*National Creative Research Initiative Center for Superfunctional Materials, Department of Chemistry, Division of Molecular and Life Sciences, and Department of Physics, Pohang University of Science and Technology, San 31, Hyojadong, Namgu, Pohang 790-784, Korea*
[2]*Department of Physics, I.I.T. Roorkee, Roorkee-247 667, India*

We investigate the pathway of thinning process for transient [110] nanowires (NWs) of Ag. The result is in good agreement with experimental observations. An unambiguous identification of the structure of a NW requires at least two views along different directions. In the cases where two views of different NW structures are practically the same for very thin NWs which pose experimental difficulty due to small signal-to-noise ratio, our theoretical analysis helps distinguish these structures. On the basis of conductance (G) calculations vis-á-vis the structure of transient NWs, the puzzling experimental observation of fractionally quantized G values is explained by considering the existence of mixed structures for thin wires.

Nanowires (NWs) are a novel organization of atoms yet to be understood and explored for the development of nanoelectrical devices with quantum conductance [1]. Relevance of atomic-size electrical contacts and conductors in the development of nanoelectronic devices [2,3] has added to the importance of NWs. These are made in several ways: e.g., by mechanically controllable break-junction experiments (MCBJE) [4]. Regular NWs along [110] are the most frequently observed among the three directions, as seen for Au, Ag, and Cu [5–7]. These [110] NWs adopted in the MCBJE have been found to undergo thinning on a time scale which allows snapshots using sophisticate devices. We have explored the pathway for the thinning process identifying the "magic structures" that the NW would adopt before breaking down. Availability of experimental data prompted us to choose Ag NWs for this study. The conductance in MCBJE [6] can be the main aspect to distinguish structures of very thin Ag NWs. Therefore, we have also studied the conductance of NWs to facilitate the inference. Our results explain all available experimental data including the fractional conductance presented during the evolution of the NW. This indicates that the structure of NWs is well identified, even for very thin NWs which defy identification due to small signal-to-noise ratio during experiments.

We carried out the density functional calculations of Ag NWs employing ultrasoft Vanderbilt-type ionic pseudopotentials with a uniform energy cutoff of 220 eV, and generalized gradient approximation for the exchange-correlation potential [8]. The initial structure of various n/m NWs was built by alternate stacking of (110) atomic planes, where n atoms are taken from one plane and m from the other. This setup of initial structures is in accordance with the experimental observations [5,6].

Figure 1(a) shows the energy profile for the average number of atoms on each cross section (N/L) of NW,

where N is the average number of atoms in a unit cell of NW and L is the length of the unit cell. For simplicity, as an alternative or equivalent representation, the horizontal axis can be given in terms of the effective radius (R) of NW, regardless of its shape (even if the cross section is far from the circular shape). R is not the real radius, but the effective radius defined as $[(N/L)\sigma_a/\pi]^{1/2}$, where σ_a is the atomic cross section. It should be noted that the energy curve is represented with respect to N/L which is unique (but not with respect to the actual radius or actual cross section which depends on the parameter). The energy profile shows which structures are more stable for the given N. As N decreases, the (slow or adiabatic) thinning process would take the most stable structure among many possible NW conformations (which are less stable than the thicker NWs) for the given N. Thus, the thinning process follows the points on the contour in Fig. 1(a). The curve was fitted to show which structures would be more stable among these points. The points above or below the curve would be less or more stable during the thinning. Figure 1(a) which shows the magic structures based on the stability of isolated NWs can be reinterpreted as Fig. 1(b) which shows the magic structures based on the stability of NWs extracted from the bulk in the case of the thinning process. The latter can be investigated from the balance of strain [produced by stretching force (f)] versus stress [restoring force due to the surface tension (τ) of NW], since the system with the NW stretched from the bulk has the extra surface area of the NW ($SL \approx 2\pi RL$, where S is the surface area per unit length of NW) with respect to the bulk system (Fig. 2).

In Fig. 2, the force f describing the generalized wire tension in drawing a NW by pulling the tips apart, from length zero to L, can be written as $f = (E - \mu_b N)/L$ [9], where E is the wire free energy in a unit cell ($= \mu N$ which equals the total energy at 0 K), and μ/μ_b is the NW/bulk
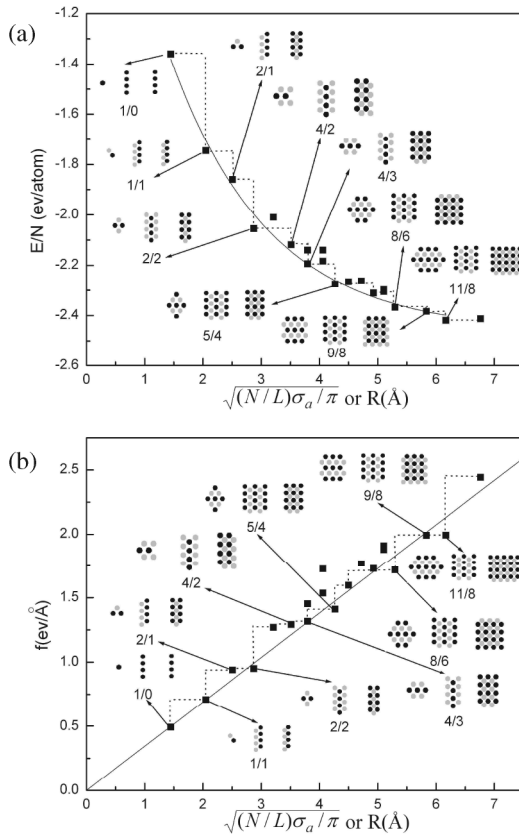
096104-1

FIG. 1. Energy vs $\sqrt{(N/L)}$ (or effective radius, R) (a) and tension vs $\sqrt{(N/L)}$ of [110] Ag NWs (b). The top view (the cross section of NW along [110]) followed by two side views (along [−110] and [001]) is shown for the well-favored (except 4/2 and 2/1) structures. The unlabeled structures (from bottom to top) are 4/1, 3/4, 6/2, 2/6, 6/4, 8/3, 6/6, 5/8, 8/5, and 15/8.

chemical potential. The surface tension of NW is $\tau = \gamma S$. From the strain-stress balance, $f = \tau = \gamma S = (\mu - \mu_b)N/L$. A tip-suspended wire would minimize this force f and hence favor the structure with smaller f in Fig. 1(b) during the thinning process. The fit of points on the contour would give the guideline about which structure would be more or less favored depending on the position below or above the fit line. In terms of the effective radius of NW, f is roughly represented as $f \approx \gamma 2\pi R$, leading to a near
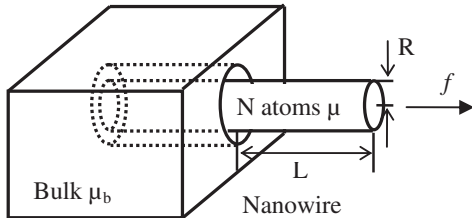

FIG. 2. Simplified picture representing the extraction of a NW from bulk.

straight line, which is exciting and reasonable. If the NW cross section is near circular, then f is close to $\gamma 2\pi R$. If it is far from the circular shape, $f > \gamma 2\pi R$, because the circular cross section would have the minimal surface tension. The smallest slope gives $\gamma = 0.8$ N/m for the 11/8 structure. The decrease in tension is the driving force behind the thinning [10] which takes place by depletion of atoms from the NW to the tips. The energy profile may possess local minima, corresponding to favorable structures during thinning of NW. It is these "magic" structures materializing during the thinning process that are sought in this study. Experimentally, thinning occurs on a time scale which is visible within seconds, and snapshots can thus be taken. It provides a direct evidence for correctness of this approach in suggesting the thinning process. Thus, from Fig. 1, the magic structures indicate metastable states which would be experimentally observable. We note that for small cross sections ($1 \leq N \leq 15$, or 1.5 Å $< R <$ 7.0 Å) considered in this work, the magic NWs are made of 11/8, (9/8), 8/6, 5/4, (4/3), 2/2, (1/1), and 1/0 structures, as shown in Fig. 3 (with not so well-favored structures in parentheses).

Experimentally, the high-resolution transmission electron microscopy (HRTEM) would reflect the projections of atoms along the observation direction. Figure 1 shows that many different structures have the same side view along [−110], e.g., (11/8, 9/8, 8/6, and 5/4 NWs) or (4/3, 4/1, and 2/2 NWs). Therefore, one side view alone is not sufficient to assign a unique identity to the structure. We find that of the 4/1 and 2/2 structures with same [−110] view, it is the 2/2 structure which is favored energetically and is, therefore, more likely to materialize during thinning process, instead of the 4/1 structure which was conjectured as a possible candidate [6]. The other side view (along [001] in Fig. 1), distinguishing the two, would help evolve an almost unambiguous inference about the structure of a NW. Interestingly, however, in some cases even these two side views may be identical (e.g., for 9/8 and 8/6 NWs) and, hence, insufficient for unique identification. In such cases, calculations like this would help resolve the identity crisis.

Another advantage of this study is that it helps identify even the structure of the ultrathin NWs, which otherwise is not easily identifiable in HRTEM observations because of the small signal-to-noise ratio in the image [6]. For example, out of the 2/1 and 1/1 structures, the ultrathin NW
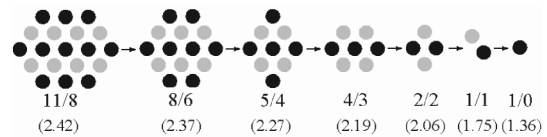

FIG. 3. Pathway (showing up the top view) of the thinning process for [110] Ag NWs. The value in parentheses are the energy per atom in eV.

[Figs. 1, 2 of Ref. [6]] was conjectured as 2/1. Our Fig. 1, however, shows that of the two, the 1/1 structure is favored more. It may be noted that the 1/1 structure was assigned in the case of Au [11].

The structures with hexagonal cross section (4/3, 8/6, and 11/8) are consistent with the schematic diagram of the Wulff construction [12] which can be used to predict the geometry of the nanoclusters. The flanks of the ultra thin NWs, 2/2 and 1/1, are composed of the (111) facets. We expect the hexagonal cross section to extend to thicker [110] NWs, with flanks as low-energy (111) and (100) facets. Considering the energetics of various structures, we conclude that the simplified pathway of thinning process for Ag [110] NWs would be from 11/8 to 8/6 to 5/4 to 4/3 to 2/2 to 1/1 to 1/0 as illustrated in Fig. 3. Other less-favored intermediate structures between two neighboring structures along the pathway may also exist but only transiently. We note that 11/8, 8/6, and 5/4 NWs have smaller f, in agreement with experimental observation [6]. The kinetic aspects of the narrowing process would be interesting. According to a recent nanoscale free electron model on the activation barrier $\Delta E \approx 0.6(h/2\pi)[\gamma/m_e]^{1/2}$ for a universal size NWs (m_e: conduction band effective mass, comparable to the free electron mass) [13], the activation barriers for the stable 11/8, 8/6, 5/4, and 2/2 structures are estimated to be 0.39 eV [which is considered to be a reasonable magnitude as a fraction of the cohesive energy per atom of the NWs that changes from 2.42 eV (11/8) to 1.36 eV (1/0)]. This gives the lifetime $\tau \approx 1$ s at $T = 150$ K and $\tau \approx 10$ μs at $T = 300$ K according to the free electron model [$\tau \approx \nu_D^{-1} \exp(\Delta E/T)$; ν_D: Debye frequency]. This value is in reasonable agreement with the experiment [6]. However, the high stability of novel metal NWs [14] could be better understood by including the effect of d electrons.

We find that with the increase in R, the spacing along [110] gradually increases as 2.83, 2.84, 2.88, and 2.90 Å (for 2/2, 4/3, 8/6, and 11/8 NWs, respectively) towards the bulk value, in agreement with shorter nearest neighbor distance in the metallic NWs and nanoclusters [15]. The rare occurrence of the monatomic (1/0) wires along [110], as compared to [111] or [100] directions [4,6], can be explained to some extent, considering the break force F (the slope at the inflection point of the binding energy curve) of [110] 1/1 and 1/0 NWs. The curves fitted with the so-called universal binding energy formula $E(x) = -\alpha(x - x_0)e^{-\beta(x-x_0)}$ [16] give F as a/e^2. The F of the 1/1 NW (0.75 eV/Å) is close to that of the 1/0 NW (0.86 eV/Å). The bond strength of the 1/1 NW is also the closest to that of the 1/0 NW. The tension for the 1/0 NW (Fig. 1) being comparable to the 1/1 NW which would exist only momentarily, would make the [110] 1/0 NWs much less observed.

To get a better insight into the thinning process *vis-á-vis* experimental results [6], we studied the conductance (G)

for the thin wires using an *ab initio* transport package based on nonequilibrium Green's function formalism and Landauer formula with single zeta polarization basis set [17]. In the Landauer formula, G can be approximated by the transmission function (T) near the Fermi energy, E_F [18]. Our G value for the 4/3, 4/2, 4/1, 2/2, 2/1, 1/1, and 1/0 structures at or around E_F is integral being 6, 5, 4, 3, 3, 2, and 1G_0, respectively. This indicates the ballistic conduction in consonance with the band structure (not presented) which shows as many bands (of s character) crossing the E_F. The d bands lie well below E_F. The experimental global histogram [6] shows peaks at 1, 2.4, and 4 + G_0. While comparing the G values of the proposed structures with the experimental data, we realize that during thinning, one structure gives way to the other. Since thinning is a transient process, a new structure might evolve before the old structure has actually fully faded away; i.e., mixed structures may exist, as also suggested by at least the peak at 2.4G_0 which does not correspond to any pure structure. Hence, the comparison of the calculated G values for pure structures of uniform cross section with the experimental data is not realistic. Smaller stability of thin NWs as compared to thick NWs indicates that the former is less likely to exhibit the G value corresponding to pure structures. Hence there is more likelihood for mixed structures to exist when the NW is thin, and we therefore feel that the experimental G values in the range 0 to 4G_0 [6] would correspond to mixed structures rather than to pure structures. Furthermore, experimentally it is necessary to use a nonzero bias to drive the current (to study G). The transport through nanostructure devices depends not only on the geometry of the nanostructure but also on the leads (including the electrodes, the contacts, the interconnecting wires, etc.) that connect the device to the external electronic circuit for measurements. Hence, comparison of the calculations for pure structures with the experiments cannot be taken too seriously, and cannot really be treated as a conclusive measure. In view of this, we studied the effect on G of this mixing of structures which simulates, in a way, the effect of electrodes.

Figure 4(a) shows one of the mixed structures which corresponds to $5/4 \times 4 - 4/3 \times 3 - 2/2 \times 3$. The $5/4 \times 3$ of both ends were used as left and right electrodes and the remaining $5/4 \times 1$ structure was included in the central part. Figure 4 explains how the lead parts can change the G values in this kind of structures. Figure 4(b) shows the conductance change according to the evolution of NW from $4/3 \times 1$ to $4/3 \times 3 - 2/2 \times 2 - 1/1 \times 3$ for two kind of leads; one is $5/4 \times 4$ structure (solid line), and the other is planar surface in the Ag [110] direction (dashed line). This will correspond to the inset of Fig. 3. in Ref. [6]. The pure 4/3 structure has G as 6G_0, while the conductance of the mixed $5/4 \times 4 - 4/3 \times N$ structure (N: integer) reduces to $\sim 5G_0$. When N changes from 1 to 3, the conductance is slightly reduced and fluctuates around
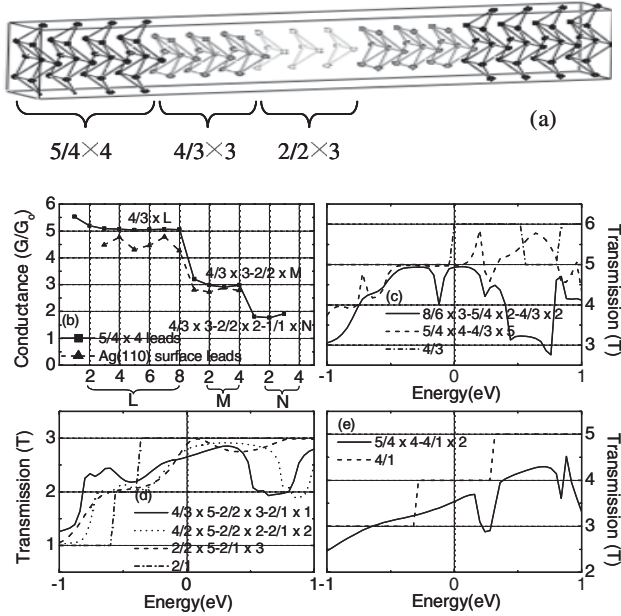
FIG. 4. (a) Example of mixed structure. The $4/3 \times 3 - 2/2 \times 3$ structure as device part is located between both leads comprised of $5/4 \times 4$ structures (b) Change of conductance during the evolution of each structure, $4/3 \times L$ ($L = 1 \sim 8$), $4/3 \times 3 - 2/2 \times M$ ($M = 1 \sim 4$) and $4/3 \times 3 - 2/2 \times 2 - 1/1 \times N$ ($N = 1 \sim 3$), between two $5/4$ leads or between two infinite planar surfaces (110). Indices L, M, and N denote the units of each structure during evolution as in (a). (c)–(e) Transmission vs energy curves for [110] NWs for pure and mixed structures. Shortened labels are used; e.g., $5/4 - 4/3$ means that both lead parts have $5/4$ structure and the central part has $4/3$ structure.

$\sim 5G_0$. After the $2/2$ structure appears in the further evolving process, the G value reduces abruptly below $3G_0$. During evolution of the $2/2$ structure, G remains almost constant. The planar surface makes the G value further reduced. The G value of $4/3$ drops to $\sim 4.5G_0$ and that of $2/2$ to $\sim 2.7G_0$. In this case, the conductance curve fluctuates more because of larger self-energy term for semi-infinite surface. This lowering trend is also observed for all mixed structures in Fig. 4 and also for other structures (not shown here). Variation of the G value in Figs. 4(c)–4(e) shows that the more mixed the structure, the smaller the G value is. Hence the effect of bigger lead is to reduce the original G value. This indicates that $4/3$ (or $4/2$), which have $6G_0$ ($5G_0$) for the pure, could be $4 + G_0$ in mixed structures, while $2/2$ and $2/1$ (with $3G_0$ for the pure) could be $2.4G_0$, as observed in the experiment [6]. The probability of occurrence of $4/1$ structure (which was once conjectured due to the same HRTEM images with that of the $4/3$ structure) is thus ruled out on the basis of its stability as well as its conductance which is $4G_0$ for pure structure and

slightly less for mixed structure [Fig. 4(e)]. In fact, for the mixed structure comprised of two layers planar surface in the lead parts and $5/4 \times 2 - 4/3 \times 1$, 2, 3 in the central part, the G value (not shown) is $\sim 4G_0$.

To conclude, we find the magic structures during the thinning of [110] Ag NWs. The $11/8$, $8/6$, $5/4$, $(4/3)$, and $2/2$ NWs appear more stable, and the hexagonal cross sections along with low energy (111) and (100) facets are favored. The structure of the electrodes is found to have a profound effect on the G value; the bigger the mixed structure, the smaller the G value is. Our results are in good agreement with the HRTEM and conductance measurements [6]. This indicates that the fractional conductance values are due to the existence of the mixed structures. The present theoretical calculations also explain the experimental observations [18] for Au NWs whose detail will be reported elsewhere.

*Corresponding authors.
†Email address: rodman@postech.ac.kr
‡Email address: kim@postech.ac.kr

[1] J. I. Pascual *et al.*, Science **267**, 1793 (1995); A. Ayuela *et al.*, Phys. Rev. B **66**, 035417 (2002); W. T. Geng *et al.*, Phys. Rev. B **67**, 233403 (2003).
[2] U. Landman *et al.*, Phys. Rev. Lett. **77**, 1362 (1996); R. N. Barnett and U. Landman, Nature (London) **387**, 788 (1997).
[3] Y.-J. Lee *et al.*, Phys. Rev. B **69**, 125409 (2004); T. Nautiyal *et al.*, Phys. Rev. B **69**, 193404 (2004); W. Y. Kim *et al.*, Phys. Rev. B **71**, 113104 (2005).
[4] A. I. Yanson *et al.*, Nature (London) **395**, 783 (1998).
[5] V. Rodrigues *et al.*, Phys. Rev. Lett. **85**, 4124 (2000); J. C. González *et al.*, Phys. Rev. Lett. **93**, 126103 (2004).
[6] V. Rodrigues *et al.*, Phys. Rev. B **65**, 153402 (2002).
[7] Y. Kondo *et al.*, Science **289**, 606 (2000); B. H. Hong *et al.*, Science **294**, 348 (2001); J. Am. Chem. Soc. **123**, 10 748 (2001).
[8] G. Kresse *et al.*, Phys. Rev. B **47**, R558 (1993); D. Vanderbilt, Phys. Rev. B **41**, 7892 (1990); J. Perdew and Y. Wang, Phys. Rev. B **46**, 6671 (1992).
[9] E. Tosatti *et al.*, Science **291**, 288 (2001).
[10] J. A. Torres *et al.*, Surf. Sci. **426**, L441 (1999).
[11] H. Ohnishi *et al.*, Nature (London) **395**, 780 (1998).
[12] L. D. Marks, Rep. Prog. Phys. **57**, 603 (1994).
[13] J. Bürki *et al.*, Phys. Rev. Lett. **95**, 090601 (2005).
[14] R. H. M. Smit *et al.*, Nanotechnology **15**, S472 (2004).
[15] C. Jo, J. I. Lee, and Y.-R. Jang, Phys. Stat. Sol. **241**, 1427 (2004); J.-C. Zheng *et al.*, Inter. J. Nanosci. **1**, 159 (2002).
[16] S. R. Bahn *et al.*, Phys. Rev. Lett. **87**, 266101 (2001).
[17] M. Brandyge *et al.*, Phys. Rev. B **65**, 165401 (2002).
[18] L. G. C. Rego *et al.*, Phys. Rev. B **67**, 045412 (2003).